Satellite-derived Sea Surface Temperatures—A Comparison between Operational, Theoretical, and Experimental Algorithms

IAN J. BARTON

CSIRO Division of Atmospheric Research, Aspendale, Victoria, Australia

(Manuscript received 13 April 1991, in final form 3 September 1991)

ABSTRACT

The Advanced Very High-Resolution Radiometers (AVHRR 2) on the National Oceanic and Atmospheric Administration (NOAA) operational meteorological satellites (currently *NOAA-11*) provide radiometric data at wavelengths of 3.7, 10.8, and 11.9 μm that enable an estimate of sea surface temperature (SST) using a differential absorption technique to allow for atmospheric effects. The operational multichannel SST (MCSST) algorithms used by NOAA/NESDIS (National Environmental Satellite, Data, and Information Service) are derived from a regression analysis of coincident satellite and buoy data. The SST algorithms can also be derived using theoretical models of infrared absorption in the atmosphere. By comparing the coefficients of operational, theoretical, and experimental algorithms it is possible both to assess the performance of the transmission models and to gain an insight into the physical processes underlying the SST algorithms.

Two sets of data are also used in this study. First, a set of coincident ship and satellite data is used to derive simple experimental multichannel SST algorithms. The second set of data, collected using two satellites with overlapping swaths, has been used to produce experimental multipath algorithms for satellite-derived SSTs.

The collective results discussed in this paper indicate that computer models of infrared transmission through the atmosphere are not yet capable of reproducing the observed satellite measurements. A better understanding of the water vapor absorption and the infrared transmission through the atmosphere is required if accurate prelaunch SST algorithms for future satellite instruments are to be derived.

1. Introduction

For reliable prediction of climate and climate change, a global numerical model must include accurate parameterization of the energy budget at the air–sea interface and an improved knowledge of atmospheric radiative absorption processes, especially for the major greenhouse gases (water vapor and carbon dioxide). For surface energy budget parameterization, accurate global measurements of the sea surface temperature (SST) and the surface wind speed are required. Satellite radiometers are now supplying SST with an accuracy of 0.7 K in midlatitudes and 1–2 K in the tropics. The international Tropical Oceans Global Atmosphere (TOGA) Program has specified an accuracy of 0.3 K in SST for useful climate applications. To attain this goal the Along-Track Scanning Radiometer (ATSR) has been built and will soon fly on the *ERS-1* satellite to be launched during 1991. This radiometer uses a novel scanning technique that will allow the sea surface to be viewed from two different angles within the space of three minutes. The scanning geometry will allow the use of differential absorption at a single wavelength to account for atmospheric effects. When combined with standard multichannel SST (MCSST) algorithms, along with low-noise radiometric measurements, an SST accuracy meeting the TOGA requirements is expected.

One of the prelaunch tasks in the ATSR program is to derive algorithms for the derivation of SST using the multipath and multichannel techniques. A first attempt at this, using a band model of infrared transmission through the atmosphere, has recently been reported by Barton et al. (1989). They derived many linear algorithms for deriving SST using between two and six brightness temperatures (the six temperatures include nadir and forward views of the same location at three wavelengths that are similar to those on the AVHRR). In this paper the performance of these early prelaunch algorithms is assessed using data from current operational satellites (the AVHRR on the NOAA satellites) and surface-based measurements of SST combined with simultaneous radiosonde profile measurements of atmospheric temperature and water vapor content. Also, AVHRR data collected at typical ATSR view angles are used to derive experimental multipath SST algorithms that are compared with those derived theoretically. These comparisons suggest that the best ATSR operational algorithms may still be determined postlaunch using a regression technique similar to that used to derive the current MCSST algorithm by NOAA/NESDIS. The major problem in the theoretical

Corresponding author address: Dr. Ian J. Barton, CSIRO, Division of Atmospheric Research, Private Bag No. 1, Mordialloc, Victoria 3195, Australia.

determination appears to be the lack of knowledge regarding the water vapor absorption in the atmospheric windows used for SST determination. If accurate prelaunch algorithms are not available, then the ATSR data will provide more accurate measurements of infrared absorption in the atmosphere. Improved parameterization of atmospheric absorption processes is also required for the successful modeling of the effects of increased concentrations of greenhouse gases.

2. Algorithm comparison method

The standard technique for deriving SST from satellite data uses differential absorption of surface-emitted infrared radiation to measure the magnitude of the atmospheric absorption. In this paper a parameter is derived that quantifies the differential absorption and thus enables a comparison of the various algorithms used to derive SST.

Several forms of algorithm exist for deriving SST from data supplied by satellite infrared radiometers. In almost all cases a linear form of algorithm is used that sometimes includes a dependence on view (satellite zenith) angle. The operational MCSST algorithm used by NOAA/NESDIS takes the form

$$\mathrm{SST} = aT_y - bT_x + c. \qquad (1)$$

Here T_y and T_x are the satellite measured brightness temperatures in channels y and x, and a, b, and c are coefficients that can include a simple linear dependence with S ($S = \sec\theta - 1$) where θ is the zenith angle of the satellite when viewed from the surface. The general form of these algorithms is such that a is approximately $(b + 1)$ and c is largely dependent on the difference between a and $(b + 1)$. In fact, many algorithms assume that $b = (a - 1)$ and then c is usually small. Thus, a simple means of comparing algorithms, and the method employed in this paper, is to use a parameter based on the coefficients a and b. Here the ratio b/a or $(a - 1)/a$ is used to describe each algorithm. This ratio is the slope of the best linear fit to a plot of the temperature deficits in the satellite radiometer channels x and y. (A temperature deficit is defined as the difference between the SST and the satellite brightness temperature, e.g., $D_x = \mathrm{SST} - T_x$.) For example, the algorithm in Eq. (1) can be rewritten as

$$D_y = (b/a)D_x + c/a + (a - b - 1)\mathrm{SST}/a, \qquad (2)$$

where the temperature deficits D are the difference between the SST and the satellite brightness temperature. The coefficients of the algorithms discussed in this paper are valid only if the satellite brightness temperatures and the derived SST are expressed in degrees absolute (K). For the *NOAA-9* daytime operational MCSST algorithm used by NOAA/NESDIS, where $a = 3.4317$, $b = 2.5062$, and $c = 21.92$, the algorithm (at SST = 290 K) reduces to

$$D_4 = 0.7303D_5 + 0.09. \qquad (3)$$

For algorithms in which the zenith angle dependence is included, the algorithm is characterized as a value of b/a at a specified zenith angle. Again, an operational MCSST algorithm is used as an example. In this case the *NOAA-11* daytime algorithm for AVHRR channels 4 and 5 gives $b/a = 0.7233$ and 0.7500 at $\theta = 0°$ and 55°, respectively.

In some regards the value of b/a can be taken as a measure of the relative atmospheric absorption in the two infrared channels. This parameter is used to compare the algorithms in the following sections. As a general guide, a variation of 0.01 in the value of b/a is equivalent to a discrepancy of about 0.5 K across a range of surface temperatures between 280 and 300 K. This is clarified in Table 1, which shows typical SST values calculated using simple linear algorithms [Eq. (1)] with a set to 3.5 and with three different values of b/a. In each case, the value of the constant c is selected to give an SST of 280 K with brightness temperatures of 278 and 277 K in the two satellite channels. The values of SST have then been calculated for brightness temperatures of 295 and 293 K, and the difference in the derived values indicates the sensitivity of the algorithms to changes in b/a.

3. Establishment of algorithms

a. *MCSST and theoretical algorithms*

The operational MCSST algorithms that have been supplied by E. P. McClain of NOAA/NESDIS give values of b/a as listed in Table 2. These values can be compared with those derived theoretically and those derived from a set of ship and satellite measurements made in the Australian region.

The theoretical values were obtained using the spectral band model of atmospheric transmission described by Barton (1985) and Barton et al. (1989). The model is based on the absorption coefficients given in the LOWTRAN-5 code and accurately calculates the emission and absorption for each of many thin atmospheric layers. It then uses a recursive procedure to determine the downcoming sky radiance as well as the upwelling radiance at the top of the atmosphere. The surface emissivity values used are calculated in the manner of Masuda et al. (1988). For each of the five-channel AVHRR instruments, values of b/a were calculated and these values are included in Table 2.

TABLE 1. Simulated values of SST (K) for algorithms with different values of b/a.

b/a	0.70	0.71	0.75
a	3.50	3.50	3.50
b	2.45	2.485	2.625
c	−14.35	−4.655	34.125
SST (T_y = 278, T_x = 277)	280.00	280.00	280.00
SST (T_y = 295, T_x = 293)	300.30	299.74	297.50

TABLE 2. Coefficients of the algorithms used in the comparison. Where applicable the values of b/a are given for satellite zenith angles of 0° and 55°. The model algorithms were derived assuming noise temperatures of 0.1 K in both the AVHRR and ATSR data. The parameter S is equal to (sec $\theta - 1$) where θ is the zenith angle of the satellite when viewed from the earth's surface.

Algorithm	Satellite	Channels	Angles	a	b	c	b/a 0°	b/a 55°
				MCSST–model comparison				
MCSST	*NOAA-7*[a]	4, 5	0–45	3.6125	2.5779	−10.05	0.714	
Model	*NOAA-7*	4, 5	0–45	3.5648	2.5649	0.34	0.720	
Model	*NOAA-7*	4, 5	0–65	3.3713 + 0.8434S	2.3659 + 0.8366S	−1.20 − 1.87S	0.702	0.747
MCSST	*NOAA-9*[b]	4, 5	0–45	3.4317	2.5062	21.92	0.730	
MCSST	*NOAA-9*[c]	4, 5	0–65	3.6037 + 0.2700S	2.6316 + 0.2700S	8.13 + 0.74S	0.730	0.744
Model	*NOAA-9*	4, 5	0–65	3.4386 + 0.8528S	2.4289 + 0.8454S	−2.07 − 1.70S	0.706	0.751
MCSST	*NOAA-11*	4, 5	0–65	3.6732 + 0.5265S	2.6570 + 0.5265S	−4.58	0.723	0.750
Model	*NOAA-11*	4, 5	0–65	3.4003 + 0.8602S	2.3932 + 0.8525S	−1.59 − 2.04S	0.704	0.749
				Ship data–model comparison				
Ship	*NOAA-9*	4, 5	0–45	3.9575	2.9575	−0.35	0.747	
Model	*NOAA-9*	4, 5	0–45	3.6377	2.6335	−0.46	0.724	
Ship	*NOAA-9*[d]	4, 5	45–65	5.4230	4.4230	−2.28		0.816
Model	*NOAA-9*	4, 5	45–65	4.1739	3.1689	−0.46		0.759
				Multipath satellite data–model comparison				
ATSR		4*N*, 4*F*		6.1350	5.1350	−2.68	0.837[e]	
Model		4*N*, 4*F*		3.1195	2.0764	−12.71	0.666[e]	
ATSR		5*N*, 5*F*		10.2041	9.2041	−9.77	0.902[e]	
Model		5*N*, 5*F*		3.6758	2.6160	−18.13	0.712[e]	
ATSR		4*F*, 5*F*		4.1920	3.1920	−0.92		0.761
Model		4*F*, 5*F*		4.0673	3.0536	−2.97		0.751

[a] McClain et al. (1985).
[b] Daytime algorithm.
[c] Nighttime algorithm.
[d] A combination of *NOAA-7* and *NOAA-9* data used.
[e] b/a for multipath (multiview angle) algorithm.

b. Algorithms from coincident ship and satellite data

Experimental algorithms were derived for coincident ship and satellite measurements obtained during four cruises in the Australian region. Two of these cruises were in tropical locations with water temperatures in excess of 27°C. Cruise details are given in Table 3. The ship measurements of SST were obtained with either an accurate thermosalinograph or a bucket thermometer and are accurate to 0.1 K.

During each cruise, satellite data were collected from the five-channel AVHRR instrument on the operational NOAA satellite. The raw satellite data were first converted to brightness temperatures using the procedures described by Lauritson et al. (1979) and then corrected for nonlinear detector characteristics (Brown et al. 1985). Navigation of the satellite data was performed using ground control points and then the brightness temperatures at the ship location were determined. Cloud observations were taken from the ship, and the satellite data were also scanned for the presence of clouds. For daytime measurements the raw data for each pixel in AVHRR channels 1, 2, 4, and 5 were checked for absolute value and uniformity over an area of 9 × 9 pixels around the ship location. For the visible channels, variations of more than one count in adjacent pixels were taken to indicate the presence of cloud. For the infrared channels the threshold was varied according to view angle and the presence of frontal structure in the SST field. This technique ensured that the satellite data used in the analysis were uncontaminated by clouds. For the night data a similar technique was used with channels 4 and 5.

Data from the first three cruises in Table 3 have already been presented by Barton et al. (1989), where they were used to investigate differences between the satellite brightness temperatures and those predicted using the band model of atmospheric transmission. Table 3 includes SST values derived using theoretical and operational (MCSST) algorithms. Generally, the model-derived values of SST are approximately 0.4–0.8 K higher than the MCSST values, and 0.3–1.0 K higher than the ship-measured SST.

From the limited amount of data in Table 3, values of b/a were calculated for a linear relation between the temperature deficits in channels 4 and 5. These experimental values are included in Table 2. The "ship" algorithm for *NOAA-9* (0°–45°) was obtained by find-

TABLE 3. Details of ship and satellite data. Temperatures are given in degrees Celsius. (Note: both the MCSST and model SST are obtained using the satellite temperatures with the appropriate algorithm).

Date	Latitude (°S)	Longitude (°E)	Ship temperature (°C)	Zenith angle (°)	Satellite temperatures		Temperature deficits 0°–45°		Temperature deficits 45°–65°		MCSST	Model SST
					T_4	T_5	D_4	D_5	D_4	D_5		
Bass Strait, July–September 1984 (*NOAA-7*)												
5 July 1984	40.77	147.92	12.6	33	9.6	8.7	3.0	3.9			11.7	12.2
8 August 1984	34.88	151.22	18.0	59	13.7	12.1			4.3	5.9	17.7	19.2
8 August 1984	36.57	150.35	15.6	27	13.6	12.6	2.0	3.0			16.1	16.4
7 October 1984	32.90	153.53	20.7	16	17.5	16.2	3.2	4.5			20.9	21.0
12 October 1984	31.58	153.90	20.3	46	18.1	17.1			2.2	3.2	20.7	21.3
13 October 1984	31.75	153.18	21.2	49	18.0	17.0			3.2	4.2	20.6	21.2
1 December 1984	38.80	148.33	16.1	26	14.6	13.6	1.5	2.5			17.1	17.4
2 December 1984	38.67	148.12	15.0	3	13.5	12.9	1.5	2.1			14.9	15.3
Coral Sea, October–November 1985 (*NOAA-9*)												
25 October 1985	18.42	153.50	26.7	50	19.9	17.7			6.8	9.0	25.7	27.3
28 October 1985	15.57	156.53	28.4	65	15.6	12.5			12.8	15.9	23.7	28.1
29 October 1985	13.37	154.93	29.2	54	19.1	16.0			10.1	13.2	27.2	29.6
31 October 1985	13.03	151.73	27.3	36	22.9	21.4	4.4	5.9			26.8	27.8
31 October 1985	13.53	150.75	27.1	5	22.5	20.7	4.6	6.4			27.1	27.7
4 November 1985	16.57	147.68	26.9	43	17.9	15.1	9.0	11.8			25.3	26.5
Indian Ocean, August–September 1987 (*NOAA-9*)												
27 August 1987	29.12	113.73	20.4	12	18.0	17.0	2.4	3.4			20.7	21.2
28 August 1987	29.12	113.87	19.9	10	17.4	16.3	2.5	3.6			20.3	20.8
28 August 1987	29.75	114.40	20.7	26	18.5	17.7	2.2	3.0			20.7	21.3
29 August 1987	28.18	113.80	19.6	29	17.1	16.1	2.5	3.5			19.8	20.5
30 August 1987	29.10	113.42	19.0	40	15.2	13.9	3.8	5.1			18.8	19.6
6 September 1987	29.07	114.45	18.8	1	16.7	15.9	2.1	2.9			18.9	19.4
7 September 1987	30.77	114.60	19.1	15	17.2	16.5	1.9	2.6			19.1	19.7
7 September 1987	31.69	115.17	19.7	36	17.7	16.9	2.0	2.8			19.9	20.7
Tropical west Pacific Ocean, May 1988 (*NOAA-9*)												
9 May 1988	3.98	150.73	30.9	35	23.6	20.9	7.3	10.0			30.6	31.6
14 May 1988	0.25	152.90	29.5	11	19.8	16.4	9.7	13.1			28.7	28.9
15 May 1988	−1.26	153.01	28.7	32	19.4	15.9	9.3	12.8			28.5	29.3

ing the line of best fit between D_4 and D_5 for all the *NOAA-9* data with low zenith angles (14 cases). For the high-angle ship algorithm both *NOAA-7* and *NOAA-9* data were used (6 cases). Obviously, far more data points are required to get definitive algorithms, but the data here are sufficient to indicate differences between the theoretical, operational, and experimental (ship) algorithms.

c. *Multipath algorithms from AVHRR data*

For a period, late in 1988, *NOAA-9* and *NOAA-11* were operating together in similar orbits. The slightly different orbital periods of the two satellites caused both the difference in equator crossing times of the two satellites to shorten slowly and the common area in overlapping swaths to also change slowly. Data from overlapping swaths were collected to enable the derivation of an SST algorithm using a multipath technique. This was done to enable a comparison with the algorithm obtained using the band model of transmission for ATSR by Barton et al. (1989). For this reason the multipath data were collected at satellite zenith angles of 0°–21.8° for a short-path measurement and angles of 52.3°–55.0° for the longer path. These are the range of satellite zenith angles for the data to be supplied by the ATSR.

At the start of the measurement period two overlapping swaths are shown in Fig. 1a. The broad bands are those areas in which the satellite zenith angle, as seen from the earth's surface, is less than 21.8°, and the narrow strips are for zenith angles between 52.3° and 55.0°. For the example shown in Fig. 1a it can be seen that data similar to that expected from the ATSR (when the broad band from one satellite overlaps the narrow band from the other) can be collected in the tropical

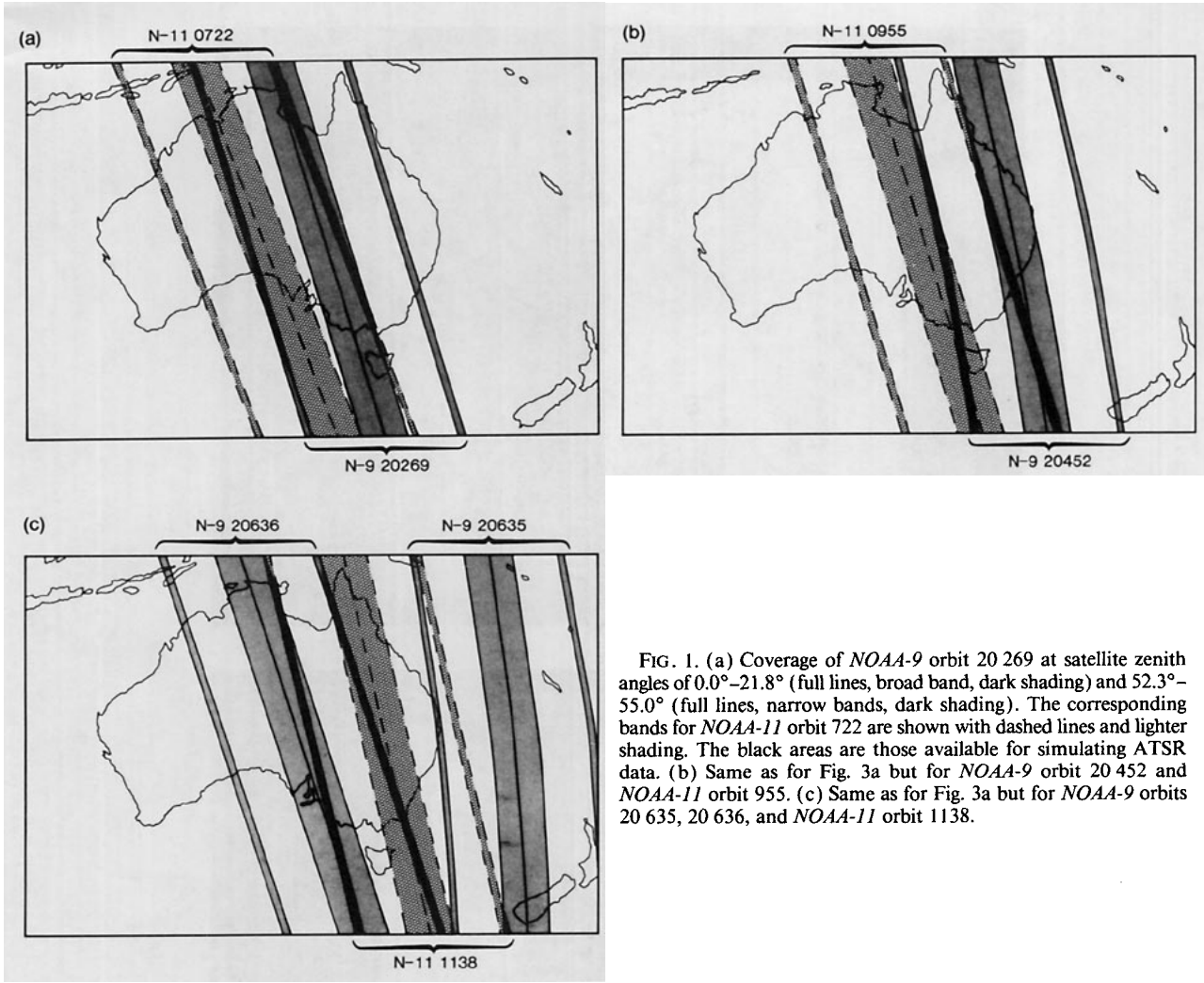

FIG. 1. (a) Coverage of *NOAA-9* orbit 20 269 at satellite zenith angles of 0.0°–21.8° (full lines, broad band, dark shading) and 52.3°–55.0° (full lines, narrow bands, dark shading). The corresponding bands for *NOAA-11* orbit 722 are shown with dashed lines and lighter shading. The black areas are those available for simulating ATSR data. (b) Same as for Fig. 3a but for *NOAA-9* orbit 20 452 and *NOAA-11* orbit 955. (c) Same as for Fig. 3a but for *NOAA-9* orbits 20 635, 20 636, and *NOAA-11* orbit 1138.

waters north of Australia. Two weeks later the areas of overlap have shifted south due to the different orbit characteristics of the two satellites (Fig. 1b). Figure 1c shows the overlapping areas late in the measurement period in which the *NOAA-9* swath (orbit 20 635) has moved through the *NOAA-11* swath (orbit 1138) and it is now the subsequent *NOAA-9* orbit that is giving the overlapping data.

Data were collected only during the daytime, as the detection of clouds was more reliable and accurate navigation using the visible channels data and coastal features was possible. The images were navigated to an accuracy of better than 2 km using at least one ground control point in the region of the overlap. To exclude any bias in the satellite measurements, the dataset included some cases when *NOAA-9* provided the short-path measurements and others when *NOAA-11* provided these data. In some of the satellite images, fine structure in the SST distribution was observed, and in these cases care was taken to sample in the same part of the SST pattern for each satellite. Figure 2 gives an example of data collected near a warm eddy in the East Australian Current. In all cases uniform areas of SST values were chosen for the analysis so that variations in the size of the footprint of the pixels at the two observation angles were not important. In two cases data were collected in which the view angle from each satellite was the same (but on opposite sides of the nadir). The good agreement obtained in these situations supported the validity of the technique of comparing measurements from the two satellites. Typical time differences between collecting the short- and long-path data were 110 min for the majority of the data but with the last four sets being nearer 200 min.

The details of the data collected are given in Table 4, and the satellite brightness temperatures are plotted in Fig. 3. In the figure the data points are joined by lines only to aid in the identification of coincident data. Full lines are used for cases when *NOAA-9* provided the short-path data and dashed lines when *NOAA-11* gave the short-path data. Also included in both the table and figure (dotted lines) are results computed

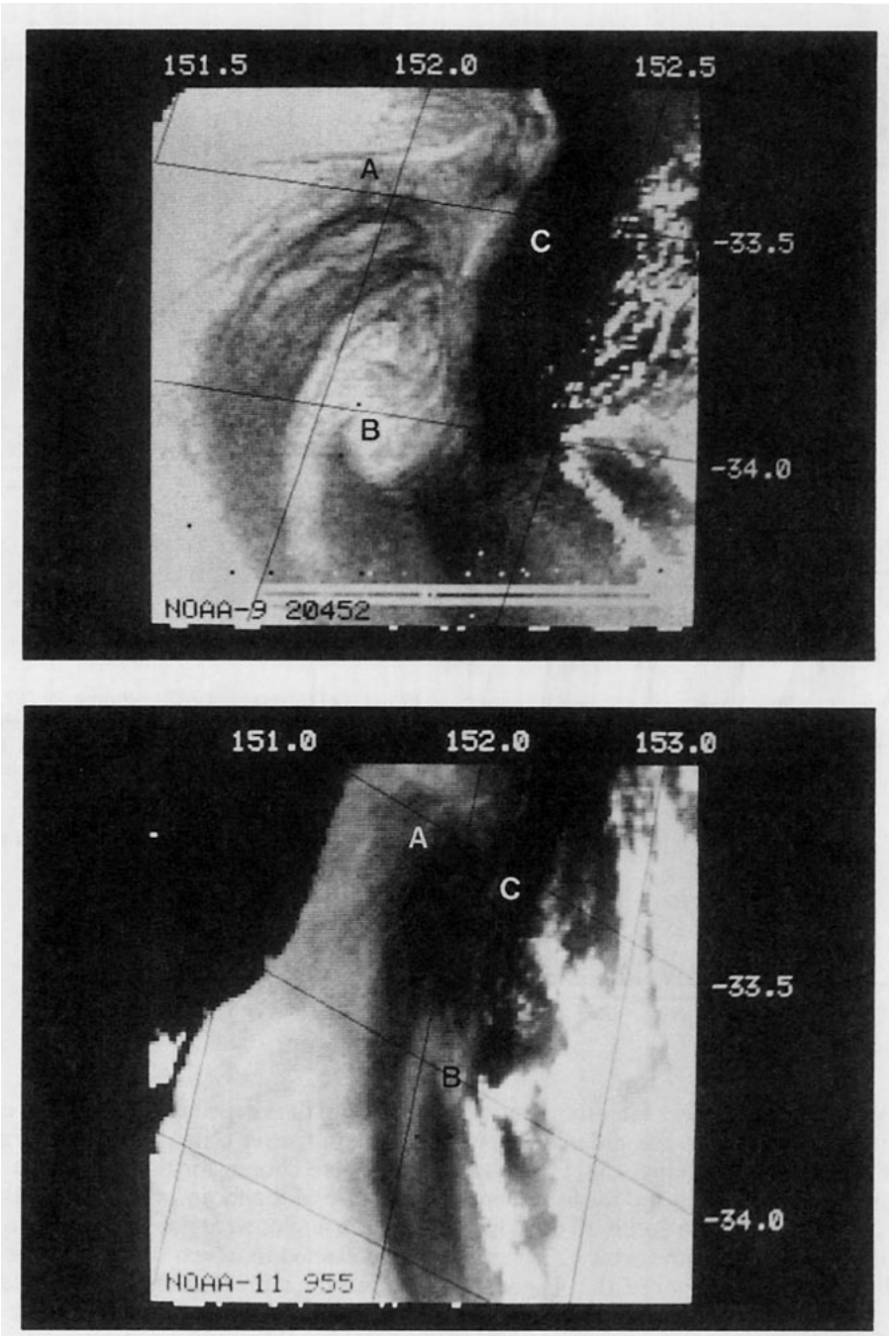

FIG. 2. AVHRR channel 4 brightness-temperature images for an area off the southeast coast of Australia. The scene includes a warm eddy of the East Australian Current and is viewed with *NOAA-9* almost overhead while the *NOAA-11* view is at a high zenith angle. The *NOAA-11* data were obtained at 0431 UTC 1 December 1988 and those for *NOAA-9* at 0619 UTC on the same day. The letters *A*, *B*, and *C* indicate locations chosen for analysis and are cross referenced in Table 3.

using the band model with the standard tropical and midlatitude summer atmospheres of McClatchey et al. (1972). Table 4 includes the MCSST calculated for both satellites.

The last four columns of the table give the temperature deficits for the four "ATSR equivalent" channels: both short and long pathlengths in AVHRR channels 4 and 5. To derive these deficits the MCSST values

TABLE 4. Multipath data collected from *NOAA-9* and *NOAA-11*. The letters, *A*, *B*, and *C* refer to locations shown in Fig. 4. The double asterisk (**) indicates data collected with the same zenith angles for the two satellites.

	Location		Short-path data					Long-path data					MCSST		Deficits			
Date 1988	Latitude (°S)	Longitude (°E)	*NOAA-X* and orbit	Time (UTC)	Zenith angle	T_4 (°C)	T_5 (°C)	*NOAA-X* and orbit	Time (UTC)	Zenith angle	T_4 (°C)	T_5 (°C)	9 (°C)	11 (°C)	D_{4N}	D_{5N}	D_{4F}	D_{5F}
18 November	15.22	138.08	9–20 269	0702	10	23.9	21.3	11–772	0500	53	21.7	18.9	30.2	29.5	6.3	8.9	8.5	11.3
22 November	39.00	150.31	11–828	0420	26**	14.5	13.3	9–20 325	0618	26	14.4	13.2	17.9	17.1	**			
25 November	20.76	157.32	9–20 367	0544	4	21.9	19.4	11–870	0350	52	19.9	17.0	28.1	27.9	6.2	8.7	8.2	11.1
29 November	34.64	136.56	11–927	0451	0	15.1	14.1	9–20 424	0641	54	13.9	12.3	18.4	17.1	2.0	3.0	3.2	4.8
29 November	34.39	136.78	11–927	0451	0	15.6	14.6	9–20 424	0641	53	14.5	12.8	19.3	17.6	2.0	3.0	3.1	4.8
30 November	36.40	151.00	9–20 438	0630	1	15.8	14.4	11–941	0441	54	14.5	12.8	19.7	19.5	3.9	5.3	5.2	6.9
30 November	35.61	150.55	9–20 438	0630	0	15.5	14.0	11–941	0441	54	14.5	12.5	19.7	19.8	4.2	5.7	5.2	7.2
1 December	33.53	151.86	9–20 452	0619	6 *A*	18.4	17.3	11–955	0431	53 *A*	17.6	16.1	21.4	21.4	3.0	4.1	3.8	5.3
1 December	34.11	152.09	9–20 452	0619	6 *B*	17.6	16.4	11–955	0431	53 *B*	16.9	15.4	20.9	20.7	3.3	4.5	4.0	5.5
1 December	33.62	152.30	9–20 452	0619	6 *C*	19.8	18.6	11–955	0431	54 *C*	18.5	16.8	22.9	23.0	3.1	4.3	4.4	6.1
2 December	36.00	155.58	9–20 466	0613	5	17.0	16.0	11–969	0421	53	16.2	14.8	19.8	19.7	2.8	3.8	3.6	5.0
2 December	35.03	155.34	9–20 466	0613	5	18.0	17.0	11–969	0421	54	16.6	15.1	20.7	20.5	2.7	3.7	4.1	5.6
2 December	31.63	153.37	9–20 466	0613	11	19.6	18.5	11–969	0421	52	18.2	16.8	22.5	21.7	2.9	4.0	4.3	5.7
9 December	36.58	139.57	11–1068	0452	15	16.8	16.1	9–20 565	0637	54	15.9	14.9	18.8	18.0	1.2	1.9	2.1	3.1
9 December	38.70	144.73	11–1068	0452	37**	16.2	15.5	9–20 565	0637	37	16.2	15.4	18.6	17.5	**			
13 December	16.47	140.19	11–1124	0412	13	24.0	21.0	9–20 622	0735	54	22.7	19.6	30.4	31.4	7.4	10.4	8.7	11.8
13 December	34.43	136.58	9–20 622	0735	4	18.0	17.4	11–1124	0412	53	16.8	15.7	19.7	19.4	1.7	2.3	2.9	4.0
13 December	37.82	136.83	9–20 622	0735	1	13.7	13.2	11–1124	0412	53	13.4	12.4	15.5	15.7	1.9	2.3	2.1	3.1
14 December	39.06	139.30	9–20 636	0718	5	14.7	14.4	11–1138	0402	55	13.9	13.3	15.9	15.0	1.2	1.5	2.0	2.6
								Standard atmospheres (model-derived values)										
Tropical			*NOAA-11*		0	22.5	21.0	*NOAA-9*		55	20.3	18.5						
Midlatitude			*NOAA-9*		0	18.2	17.4	*NOAA-11*		55	16.8	15.6						

calculated using the short-path data were taken as the true SSTs. These deficits were then used to produce experimental ATSR algorithms using the same method as for the ship algorithms. Details of these algorithms are included in the last section of Table 2.

4. Algorithm comparisons

In a recent paper Schluessel et al. (1990) have discussed the impact of bulk skin-temperature differences on the determination of SST from satellite data. It is relevant to note that the theoretical algorithms used here produce a skin temperature at the top of the sea surface, while the experimental and operational algorithms are tuned to give a measure of the bulk SST beneath the surface. In the analysis undertaken in this paper, any bulk skin-temperature difference will not be significant in that it will contribute only to the value of the constant c and will not affect the differential absorption at the two wavelengths represented by b/a.

a. MCSST–model algorithms comparison

Table 2 shows that there is reasonable agreement between the operational (MCSST) and theoretical (model) algorithms. For the cases when the zenith-angle dependence is included in the algorithm, the theoretical values of b/a tend to be lower by about 0.02 for near-nadir viewing but similar for angles near 55°. As shown in Table 1, this difference in b/a is equivalent to differences in SST of near 1 K when the algorithms are used over a broad range of surface temperatures. The theoretical values for the three AVHRR instruments are all approximately equal, but are somewhat spread for the operational algorithms. In the theoretical algorithms, any differences in the values of b/a are due solely to the different spectral characteristics of the filters in each AVHRR instrument. The spread in the values of b/a for the different instruments is much greater in the operational algorithms than in the theoretical algorithms. This suggests that the frequency dependence of the absorption coefficients used in the model may not be accurate.

Because the two sets of algorithms for AVHRR channels 4 and 5 have similar coefficients (and similar values of b/a), they give quite good agreement in derived SST. This also implies that the ratio of absorption (or the differential absorption) in these two channels is reasonably correct in the model calculations, but the absolute values of the absorption coefficients may still be in error. The results reported by Barton (1990) suggest that, to accurately model observed ship and satellite measurements, the absorption coefficient in channel 5 needs to be increased by a larger factor than that in

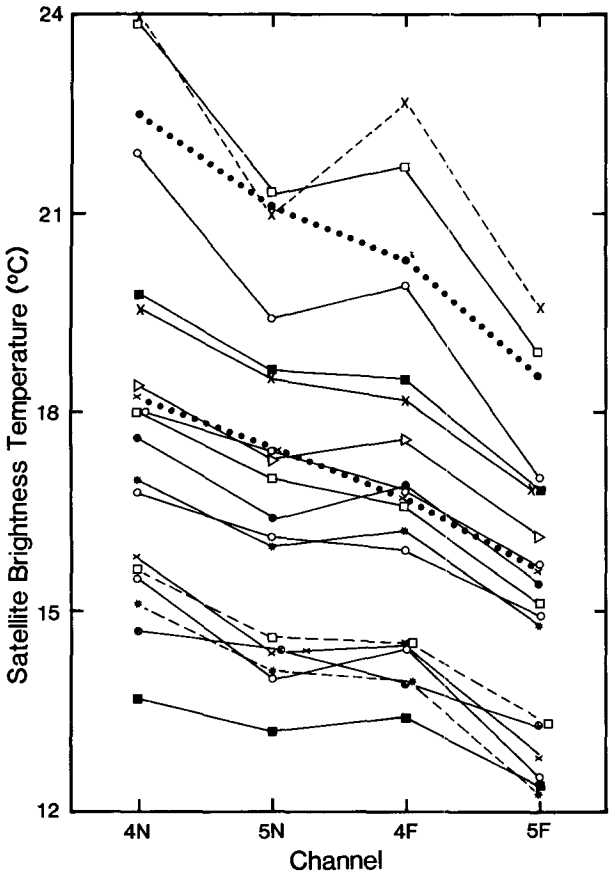

FIG. 3. Brightness-temperature values for the set of data from overlapping passes of *NOAA-9* and *NOAA-11*. The lines joining the four brightness temperatures at each location are used to portray their relative magnitude. The full lines are for data in which *NOAA-9* supplied the short-path data (4*N* and 5*N*) and *NOAA-11* the long-path data (4*F* and 5*F*) and the dashed lines vice versa. The dotted lines are for model values obtained for the standard tropical and midlatitude atmospheres of McClatchey et al. (1972).

channel 4. For the theoretical algorithms this would increase the differential absorption in the two channels and cause b/a to decrease. Then the theoretically derived algorithms would be significantly different from those used operationally. These anomalies again suggest that models can reproduce the gross features of atmospheric transmission, but cannot accurately represent the differential absorption as required for good SST algorithms.

b. Ship–model algorithm comparison

The experimental algorithms derived using the ship data have been obtained with only a small amount of data (see Table 3) and thus may have large errors. For low zenith angles the agreement is reasonable, with the ship value of b/a being 0.023 larger than the model. However, for large zenith angles, the agreement is not good. Admittedly, there is only a small amount of data, and there is a combination of data from two different instruments, but the large values of b/a at high zenith angles are also found in the analysis of overlapping satellite data.

c. Multipath algorithms comparison

The data collected from overlapping swaths of the *NOAA-9* and *NOAA-11* satellites give a good comparison of the SST products from the two satellites. Figure 4 shows the MCSST values for each coincident set of data. When comparing these data it must be noted that the *NOAA-9* algorithm does not include a dependence on scan (or zenith) angle, while the *NOAA-11* algorithm does. For the locations where the viewing angles were identical the *NOAA-9* value was higher than that for *NOAA-11*, and this was also true for the data when *NOAA-9* provided the long-path data in the midlatitudes. This difference could be due to the effect of not including an angle correction in the MCSST algorithm, especially for the long-path *NOAA-9* data. Good agreement is obtained when *NOAA-11* supplied the long-path data, even for tropical SST values.

In all cases the *NOAA-9* data were obtained 2 or 3 h later in the afternoon than the *NOAA-11* data. The effect of having a slightly cooler atmosphere was investigated using the transmission model. For typical midlatitude profiles, an atmosphere that is cooler by 2 K below a height of 1000 m gives brightness temperatures that are lower by 0.2 K, but the derived SST shows negligible change. For the bulk of the data in Fig. 3, this effect on the brightness temperatures ac-

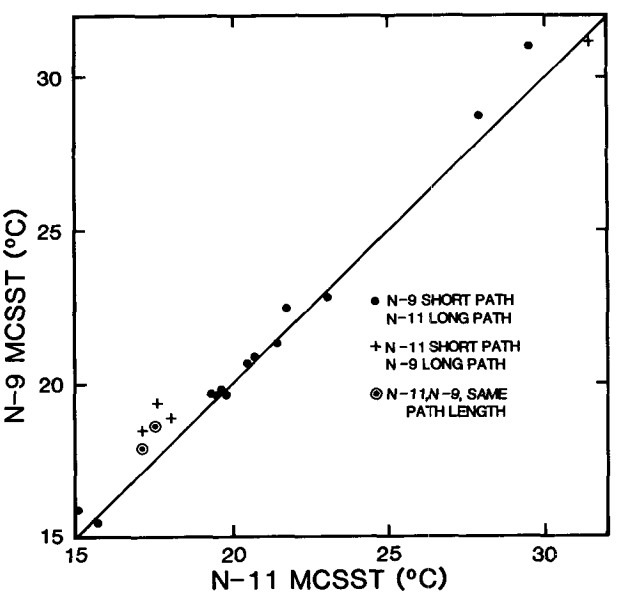

FIG. 4. *NOAA-9* and *NOAA-11* MCSST values for the set of data with overlapping passes.

centuates the (short-path channel 5)–(long-path channel 4) difference.

The relative magnitudes of the satellite-measured brightness temperatures for each location were compared by plotting their values in Fig. 3. The figure also includes values derived using the transmission model with standard atmospheres. As expected, the brightness temperatures for channel 4 are higher than for channel 5 and the short-path values at each location are higher than the long-path values. Of particular interest is the comparison between the values for the short-path channel 5 and the long-path channel 4. In almost all cases, and especially for the tropical locations, the short-path channel 5 temperature is higher than that for the long-path channel 4, while the model results show the opposite result. This supports the concept that, to improve the modeling results, a larger increase in the channel 5 absorption coefficient is required compared to that in channel 4. Alternatively, the model may be treating poorly the transmission at high zenith angles.

The multipath results may also be used to compute dual-path experimental algorithms similar to those to be used to derive SST from ATSR data. Table 3 includes the temperature deficits for channels 4 and 5 short- and long-path data. The deficits for channel 4 are plotted in Fig. 5, and the line of best fit defines an SST algorithm for dual-path data. The slope of this line is obviously b/a, and for this experimental algorithm its value is 0.837. The SST algorithm is

$$\mathrm{SST} = 6.135T_{4N} - 5.135T_{4F} - 2.95.$$

This is quite different from that derived using the technique described by Barton et al. (1989), namely,

$$\mathrm{SST} = 3.119T_{4N} - 2.076T_{4F} - 12.71,$$

which has a value of 0.666 for b/a. The theoretically derived algorithm is also shown in Fig. 5. The difference in b/a for the two algorithms is equivalent to calculated SST differences of more than 5 K when the algorithms are applied to a wide range of surface temperatures (see Table 1).

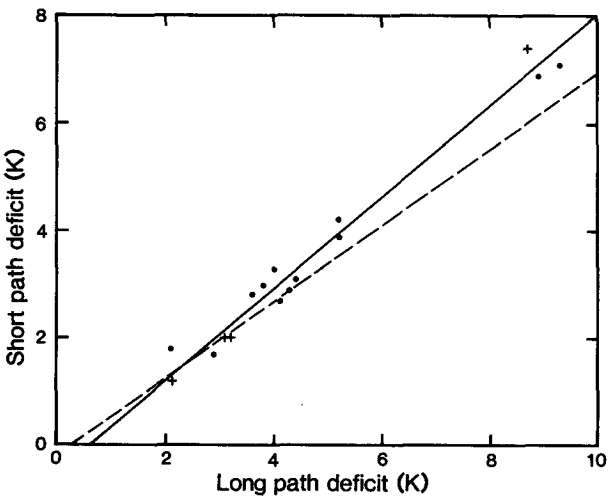

FIG. 5. Relationship between the short-path and long-path deficits for channel 4. The full line is the line of best fit, and the slope and intercept define a simple experimental SST algorithm. For comparison a dashed line representing a theoretically derived algorithm (Barton et al. 1989) is included.

5. Conclusions

The emission and absorption of infrared radiation by the atmosphere is an important physical process in the parameterization of radiative transfer in numerical models of weather and climate. The comparisons between operational, theoretical, and experimental algorithms reported in this paper show that accurate modeling of absorption in the atmospheric transmission windows is not yet possible. Also, as these windows are used by satellite radiometers to view the earth's surface, it is not yet possible to accurately correct for the effect of atmospheric absorption. This limits the usefulness of much satellite data. In particular, the measurement of SST from space cannot be accurately modeled. All the SST operational algorithms are derived from comparison between buoy and satellite data. For land surface temperatures this is not a viable technique as the emissivity of the surface is not well known (as it is for the sea surface). To enable a better use of infrared data over land surfaces it will be necessary to improve our knowledge of the nature of the atmospheric water vapor absorption.

Finally, the marked disagreement between the SST algorithms derived from satellite data and those obtained from the modeling of atmospheric absorption highlights these problems. Unless there is an improvement in the agreement between operational and theoretical algorithms, it will not be possible to obtain reliable prelaunch SST algorithms for the ATSR data. For this reason an extensive series of SST validation campaigns is planned for the immediate *ERS-1* postlaunch period. On a positive note, a combined ATSR and SST validation dataset may give a more precise determination of the atmospheric absorption coefficients and an improved understanding of radiative processes important in climate modeling.

REFERENCES

Barton, I. J., 1985: Transmission model and ground-truth investigation of satellite-derived sea surface temperatures. *J. Climate Appl. Meteor.*, **24**, 508–516.

——, 1991: Infrared continuum water vapor absorption coefficients derived from satellite data. *Appl. Opt.*, **30**, 2929–2934.

——, A. M. Zavody, D. M. O'Brien, D. R. Cutten, R. W. Saunders, and D. T. Llewellyn-Jones, 1989: Theoretical algorithms for satellite-derived sea surface temperatures. *J. Geophys. Res.*, **94**, 3365–3375.

Brown, O. B., J. W. Brown, and R. H. Evans, 1985: Calibration of Advanced Very High Resolution Radiometer infrared observations. *J. Geophys. Res.*, **90**, 11 667–11 677.

Finger, G., and F. K. Kneubühl, 1984: Spectral thermal infrared emission of the terrestrial atmosphere. *Infrared and Millimetre Waves,* 12, Part II, K. J. Button, Ed., Academic Press, 145–193.

Grant, W. B., 1990: Water vapor absorption coefficients in the 8–13-μm spectral region: A critical review. *Appl. Opt.,* **29,** 451–462.

Kneizys, F. X., J. H. Chetwynd, R. W. Fenn, E. P. Shettle, L. W. Abreu, R. A. McClatchey, W. A. Gallery, and J. E. A. Selby, 1980: Atmospheric transmittance/radiance; computer code LOWTRAN-5. Rep. No. AFGL-TR-80-0067, Air Force Geophysics Laboratory, Hanscom AFB, MA, 233 pp.

Lauritson, L., G. J. Nelson, and F. W. Porto, 1979: Data extraction and calibration of *TIROS-N*/NOAA radiometers. NOAA Tech. Memo. NESS 107, U.S. Dept. of Commerce, Washington, D.C., 73 pp.

McClain, E. P., W. G. Pichel, and C. C. Walton, 1985: Comparative performance of AVHRR-based multichannel sea surface temperatures. *J. Geophys. Res.,* **90,** 11 587–11 601.

McClatchey, R. A., R. W. Fenn, J. E. A. Selby, F. E. Volz, and J. S. Garing, 1972: Optical properties of the atmosphere. 3d ed. Rep. No. AFCRL-72-0497, Air Force Cambridge Research Laboratories, MA.

Masuda, K., T. Takashima, and Y. Takayama, 1988: Emissivity of pure and sea waters for the model sea surface in the infrared window regions. *Remote Sens. Environ.,* **24,** 313–329.

Roberts, R. E., J. E. A. Selby, and L. M. Biberman, 1976: Infrared continuum absorption by atmospheric water vapour in the 8–12 μm window. *Appl. Opt.,* **15,** 2085–2090.

Schluessel, P., W. J. Emery, H. Grassl, and T. Mammen, 1990: On the bulk skin temperature difference and its impact on satellite remote sensing of sea surface temperature. *J. Geophys. Res.,* **95,** 13 341–13 356.

Shettle, E., and R. W. Fenn, 1979: Models for the aerosols of the lower atmosphere and the effects of humidity variations on their optical properties. Air Force Geophysics Laboratory Rep. No. AFGL-TR-79-0214, 94 pp.